Published in final edited form as:
Nucl Med Biol. 2007 April ; 34(3): 267–272.

BIODISTRIBUTION AND PET IMAGING OF [^{18}F]-FLUOROADENOSINE DERIVATIVES

Mian M. Alauddin[*], **Antranik Shahinian**, **Ryan Park**, **Michael Tohme**[$], **John D. Fissekis**, and **Peter S. Conti**
Department of Radiology, PET Imaging Science Center, University of Southern California, Los Angeles, CA, USA

Abstract

Introduction: Many fluorinated analogues of adenosine nucleoside have been synthesized and studied as potential antitumor and antiviral agents. Earlier we reported radiosynthesis of 2′-deoxy-2′-[^{18}F] fluoro-1-β-D-arabinofuranosyl-adenine ([^{18}F]-FAA) and 3′-deoxy-3′-[^{18}F]fluoro-1-β-D-xylofuranosyl-adenine ([^{18}F]FXA). Now we report their in vivo studies including blood clearance, biodistribution and micro-PET imaging in tumor-bearing nude mice. Methods: Tumors were grown in six weeks old athymic nude mice (Harlan, Indianapolis, IN) by inoculation of HT-29 cells, wild type cells in the left flank and transduced cells with HSV-tk on the right flank. When the tumor was about 1 cm in size, animals were injected with these radiotracers for *in vivo* studies, including blood clearance, micro-PET imaging and biodistribution. Results: Uptake of [^{18}F]FAA in tumor was 3.3-fold higher than blood, with highest uptake in the spleen. Maximum uptake of [^{18}F]FXA was observed in the heart compared to other organs. There was no tumor uptake of [^{18}F]FXA. Biodistribution results were supported by micro-PET images, which also showed very high uptake of [^{18}F]FAA in spleen and visualization of tumors, and high uptake of [^{18}F]FXA in the heart. Conclusion: These results suggest that [^{18}F]FAA may be useful for tumor imaging, while [^{18}F]FXA may have potential as a heart imaging agent with PET.

Keywords

[^{18}F]-FAA; [^{18}F]-FXA; adenosine; micro-PET

INTRODUCTION

Many fluorinated analogues of adenosine nucleoside have been synthesized and studied as potential antitumor and antiviral agents [1–11]. Among these, 2′-deoxy-2′-fluoro-2-chloro-9-β-D-arabinofuranosyl-adenine has been found to be active against human colon tumor xenografts [6,7]. The 2′-deoxy-2′-fluoro-arabino compounds gained much attention as anticancer agents [6–8], and the 3′-deoxy-3′-fluoro-ribo compounds have shown antiviral activity [9–11]. However, little information is available regarding the biological properties of the xylo-derivative, 3′-fluoro-9-β-D-xylofuranosyl-adenine [1,12,13]. Most recently [^{14}C]-adenosine has been shown to be a marker for myocardial blood flow in dogs [14]. A synthesis

Address correspondence to: Mian M. Alauddin, Ph.D., 1515 Holcombe Blvd. T8.3895, Box 059, Houston, TX 77030, Phone: 713-563-4872, Fax: 713-563-4894, E-mail: alauddin@di.mdacc.tmc.edu
[*]Present address: Department of Experimental Diagnostic Imaging, University of Texas MD Anderson Cancer center, Houston, TX
[$]Current address: Department of Biomedical Engineering, UC Davis, Davis, CA

of [^{11}C]-adenosine monophosphate has been reported in order to investigate its potential use for imaging tumor with PET [15]. [^{18}F]-Labeled analogues of adenosine, particularly those that are non-catabolized, also have potential for PET imaging of cell proliferation and/or viral infection.

We have been exploring the radiofluorination of furanosyl pyrimidine derivatives as potential agents for imaging cell proliferation and gene expression using PET [16,17]. We have also begun to explore radiofluorination of furanosyl purines. One synthesis of 2′-deoxy-2′-fluoro-9-β-D-arabinofuranosyl-adenine is a three step procedure and involves the incorporation of fluorine in the *arabino* configuration at C-2 of the sugar, which then is converted to its 1-bromo-derivative and coupled with the protected purine base [2,18]. An alternative approach involves the direct fluorination of an appropriate precursor of the nucleoside with various fluorinating agents followed by de-protection of the reacting intermediate [4,8]. The direct fluorination of the purine nucleoside appears to be convenient and superior to the three-step method. This contrasts our experience within the pyrimidine series where the direct fluorination fails to provide the desired product [4,15,17].

The high yield synthesis of 2′-deoxy-2′-fluoro-9-β-D-arabinofuranosyl-adenine involves treatment of N^6,3′,5′-tri-trityladenosine with (diethylamino)-sulfur trifluoride (DAST) [4, 13]. DAST is not a suitable reagent for radiochemical synthesis of these compounds due to the unavailability of the ^{18}F-labeled reagent and the required long reaction time 6–16h. A direct synthesis of [^{18}F]-labeled FAA involves the fluorination of a 2′-tosylate of a protected 9-β-D-ribofuranosyladenine [8]. However, this synthesis was reported without detailed characterization of the product. We have developed a method for the radiosynthesis of 2′-deoxy-2′-[^{18}F]fluoro-9-β-D-arabinofuranosyladenine ([^{18}F]FAA) and 3′-deoxy-3′-[^{18}F]fluoro-9-β-D-xylofuranosyladenine ([^{18}F]FXA) with complete characterization of these compounds including precursors and intermediates [18]. In this paper we report biodistribution and micro-PET imaging studies of [^{18}F]FAA and [^{18}F]FXA in tumor-bearing nude mice.

MATERIALS AND METHODS

Synthesis of [^{18}F]FAA and [^{18}F]FXA: These radiotracers were prepared following a method of direct fluorination on purine nucleoside developed in our laboratory [18]. Briefly, adenosine was converted to its N^3,2′,5′- and N^3,3′,5′-tri-methoxytrityl derivatives as a mixture. After separation, these derivatives were converted to their respective 2′- and 3′-triflates. Each triflate was reacted with tetrabutylammonium[^{18}F]fluoride to produce the corresponding 2′-arabino and 3′-xylo [^{18}F]-fluoro-derivatives. The protected fluoro-derivatives yielded the desired products by acid hydrolysis. Crude preparations were purified by HPLC to obtain the desired pure products using 9% MeCN/H_2O solvent system. The solvent was evaporated in a rotary evaporator and the products were reconstituted in saline. The resulting solutions were passed through a 0.22 micron Millipore filter and collected into a sterile apyrogenic vial. Sterility and pyrogenicity tests were performed on the final preparations after the radioactivity had decayed. Pyrogenicity test was performed using LAL reagent and *E. coli* endotoxin type 055:B5, and sterility test was performed using thioglycollate and trypticase media.

In vivo studies

Animal studies were performed under an approved USC Institutional Animal Care and Use Committee (IACUC) protocol. Tumors were grown in six weeks old athymic nude mice (Harlan, Indianapolis, IN) by inoculation of approximately 5 million cells (non-transduced) under the skin in the left flank and 8 million cells (transduced with HSV-tk) on the right flank. When the tumor was about 1 cm in size, animals were used for *in vivo* studies, including blood clearance, micro-PET imaging and biodistribution.

Blood clearance studies were conducted through a 2h time period, and biodistribution were performed at 2 hours post-injection. One group of mice (n = 5) were injected intravenously via a tail vein with the radiotracer [^{18}F]FAA (~740 MBq, 20 μCi, 200 μL). Another group of mice were injected similarly with [^{18}F]FXA (~ 740 MBq, 20 μCi, 200 μL). Activity injected into each mouse was measured in a dose calibrator (Capintec). Blood samples were taken using a capillary tube (1.33 μL) from the contralateral tail vein after rupture with a needle at different time intervals (1, 2, 5, 10, 20, 40, 60 and 120 min). Activity in each blood sample was measured in a Cobra II auto gamma counter (Packard Inst., Meriden, CT), standardized for injected dose, and percent injected dose per gram (%ID/g) was calculated. Mean % ID/g was plotted against time to obtain the blood clearance curve for each compound.

For biodistribution studies, animals were anesthetized with Nembutal (40 mg/kg) and sacrificed at 2 h post-injection. All organs including tumor were separated and weighed. Radioactivity in each organ was measured using a gamma counter and radioactivity uptake was expressed as % ID/g and organ to blood ratio. Mean uptake (%ID/g) for each group of animals was calculated with standard deviation. Statistical significance was based on two-tailed *t*-test.

For PET imaging, animals were injected with either [^{18}F]FAA or [^{18}F]FXA approximately 0.2 mCi activity through tail vein. PET imaging (10 min static scans) was performed using a Micro-PET scanner (Concorde Microsystems, Inc.), with 120 transaxial planes and spatial resolution of 1.2 mm, at 30 min, 1h and 2h post-injection at the USC PET imaging science center. Images were reconstructed using ordered subset expectation maximization (OSEM) algorithm. Regional radioactivity concentrations (KBq/cc) for [^{18}F]FAA were estimated from the maximum pixels within regions of interest drawn around the tumor or organ on trans-axial slices of the reconstructed image sets. Similarly radioactivity concentration (KBq/cc) of [^{18}F] FXA in the heart was estimated from the maximum pixels within regions of interest drawn around the heart on trans-axial slices of the reconstructed image sets. The radioactivity uptake in tumor, heart and other organs (KBq/cc, μCi/cc) was converted to %ID/g and compared with the biodistribution data.

RESULTS AND DISCUSSION

Radiotracers were prepared following a method developed in our laboratory [18]. The radiochemical yields were 10–12% decay corrected (d. c.) for [^{18}F]FAA and 30–35% (d. c.) for [^{18}F]FXA. For both compounds the radiochemical purity was > 99% and the specific activity was > 74 GBq/μmol at the end of synthesis (EOS). Sterility and pyrogenicity tests showed that all preparations were sterile and pyrogen free, suggesting that these compounds can be routinely produced in good yields and under sterile and apyrogenic conditions for animal and human studies.

These two new radiotracers have been tested in tumor-bearing nude mice in order to identify them as potential PET imaging agents for tumor proliferation and/or viral gene expression. Since fluorinated analogues of adenosine, particularly, the 3′-deoxy-3′-fluoro-ribo compounds have shown antiviral activity [9–11], we have evaluated both compounds in human colon cancer xenografts produced by inoculation of wild type cells and stably transduced cell with HSV1-tk gene in nude mice. The data generated from this study suggests that none of these compounds are substrate for HSV-tk gene, on the other hand, one compound appears to be a marker for tumor proliferation and the other compound may be a heart imaging agent.

Figure 1 represents the blood clearance of the radiotracers. From the clearance curve it appears that both compounds have a similar clearance pattern, and they clear rapidly from the blood within 20 min post-injection, then the clearance slows down. The plasma half-life ($t_{1/2}$) of

[^{18}F]FAA was approximately 10 min, while that of [^{18}F]FXA approximately 8 min, slightly lower. This difference in the plasma half-life of these compounds is within the experimental error, and may not be statistically significant. The fast blood clearance may have some advantage such as the circulating activity may be reduced within short time to produce less back ground in PET images. However, the clarity of the image also depends on the accumulation of the tracers into a specific organ of interests, which depend on longer circulation time. Compared to other pyrimidine analogues developed in our laboratory, the blood clearance appears to be similar and comparable. Table 1 represents the biodistribution of [^{18}F]FAA and [^{18}F]FXA in tumor-bearing animals at 2h post-injection. The biodistribution result shows that % ID/g of [^{18}F]-FAA in spleen, liver and kidney were high, 11.65%, 2.4% and 3.5%, respectively. Uptake of [^{18}F]-FAA in tumors was 1.75% and 1.55% of the injected dose/g in wild type and tk-positive tumors, respectively. Activity in blood and muscle was 0.53% and 0.75%, respectively. Tumor uptake was 3.3-fold higher compared to the blood activity (0.53% ID/g) and 2.3-fold higher compared to muscle, which suggests that [^{18}F]FAA may be a potential tumor imaging agent. Uptake in other organs such as heart, lung, stomach and intestine was also high. Heart is known to have a high level of adenosine receptors, therefore, it may be possible that this analogue, [^{18}F]FAA may have some affinity for the adenosine receptor. High accumulation of FAA in the spleen is most interesting. About 12% ID/g of [^{18}F]-FAA was in the spleen, which is the highest incorporating tissue. Specific accumulation of [^{18}F]-FAA in spleen suggests that the target may have some specific receptors for this compound. Further studies will be necessary to understand this high uptake in spleen. High uptake in liver and kidney indicates hepatobiliary and renal clearance of the compound.

The biodistribution of [^{18}F]FXA was quite different from that of [^{18}F]FAA (Table 1). Uptake of [^{18}F]FXA in the heart was 8.4% ID/g and that in the liver and kidney was 6.9% ID/g and 6.4 %ID/g, respectively. Uptake in other organs including blood and muscle was relatively much lower. Tumor uptake in wild type cells was 0.67% ID/g and that in the transduced cells was 0.49% ID/g. The highest uptake of [^{18}F]FXA was in the heart. High uptake in the heart indicates that this compound may have similar receptor binding property as adenosine or another type of receptor may be present in the heart for which [^{18}F]FXA is a substrate. Further studies are necessary to better understand the mechanism of uptake of [^{18}F]FXA in the heart. Compared to the activity in the blood, muscle uptake was slightly higher. [^{18}F]FXA shows much higher uptake in liver and kidneys compared to [^{18}F]FAA suggesting that the compound undergoes through hepatobiliary and renal clearance. Interestingly, there was no significant uptake of [^{18}F]FXA in tumors. The tumor/blood ratio was less than 1, suggesting that this compound is not a tracer for tumor imaging.

The biodistribution data for [^{18}F]FAA and [^{18}F]FXA are presented in the graphical form for quick and easy representation in figure 2A, B. From this graphical representation it is clearly observed that accumulation of [^{18}F]FAA into spleen is much higher than any other organs and blood, and both tumors have higher uptake than blood (Fig. 2A). Uptake in kidney and liver is also quite higher than that in blood. On the other hand, [^{18}F]-FXA has totally different biodistribution (Fig. 2B). Maximum activity of FXA is incorporated in the heart. Tumor activity of FXA is lower to that in blood. Uptake in liver and kidney is very high, which suggests hepatobiliary and renal clearance of the compound. In order to investigate these tracers as substrate for HSV-tk, we have used both transduced and non-transduced cells, HT-29, to grow tumors in the same animals. The biodistribution results suggest that these compounds are not substrates for HSV-tk.

Figure 3 represents micro-PET images of [^{18}F]FAA. Figures 3A, 3B, and 3C are coronal images at 30 min, 1h and 2h post-injection. As the images show, maximum activity is accumulated into the spleen, which is in agreement with the biodistribution data. Tumors in both flanks (wild type on the left and transduced on the right) are visible, and have similar uptake,

suggesting that this compound may be a potential tumor imaging agent. There is no significant difference in images at early and later time points suggesting that wash out of activity from the organs with time was minimal, i.e. the activity accumulated in the tissue or tumor within 30 min is retained with time.

Figure 4 represents micro-PET images of [^{18}F]FXA. Figure 4A, 4B and 4C are transaxial, coronal and sagittal images of the heart, respectively, at 2h post-injection. In the coronal and sagittal images activities are also observed in other organs and tissues in addition to the heart. However, the transaxial PET image clearly suggests that [^{18}F]FXA derived activity is in the heart and this activity did not wash out in 2h post-injection. These images are also in agreement with the biodistribution results.

From the examination of both biodistribution and micro-PET images it appears that these two compounds [^{18}F]FAA and [^{18}F]FXA have totally different but interesting pharmacokinetics. This preliminary studies of these compounds in tumor-bearing animals indicate that none of these compounds are substrate for HSV-tk. [^{18}F]FAA appears to be moderate tracer for tumor imaging while [^{18}F]FXA is not. Our findings also suggest that [^{18}F]FAA posses the hitherto unknown property of high accumulation in the spleen. Further study is required to understand the mechanism and nature of this phenomenon. [^{18}F]FXA on the other hand appears to be a good substrate for accumulation in the heart. Again further studies are necessary to understand the mechanism of heart uptake; however, in these preliminary studies [^{18}F]FXA appears to be a potential heart-imaging agent by PET. In comparison, [^{18}F]FXA has much higher hepatobiliary and renal clearance compared to [^{18}F]FAA.

CONCLUSION

[^{18}F]FAA and [^{18}F]FXA have been evaluated in tumor-bearing nude mice including blood clearance, biodistribution and micro-PET imaging. *In vivo* biodistribution and PET imaging results suggest that [^{18}F]FAA may be useful for tumor imaging, while [^{18}F]FXA may have potential as a heart imaging agent with PET.

Acknowledgements

This work was supported by the National Cancer Institute Grant CA 72896.

References

1. Right JA, Taylor NF. Fluorocarbohydrates part XVIII. 9-(3-deoxy-3-fluoro-β-D-xylofuranosyl) adenine and 9-(3-deoxy-3-fluoro-α-D-arabinofuranosyl)adenine. Carbohydrate Res 1968;6:347–354.
2. Right JA, Taylor NF, Fox JJ. Synthesis of 2-deoxy-2-fluoro-D-arabinose and 9-(2-deoxy-2-fluoro-α- and β-D-arabinofuranosyl)adenine. J Org Chem 1969;34:2632–2636. [PubMed: 5803811]
3. Ikehara M, Maruyama T, Miki H. Studies of nucleosides and nucleotides-LXXIV; Purine cyclonucleoside-34; A new method for the synthesis of 2′-substituted 2′-deoxyadenosine. Tetrahedron 1978;34:1133–1138.
4. Pankiewicz KW, Krzeminski J, Ciszeski LA, Ren WY, Watanabe KA. A synthesis of 9-(2-deoxy-2-fluoro-β-D-arabinofuranosyl)adenine and hypoxanthine. J Org Chem 1992;57:553–559.
5. Montgomery JA, Shortnacy-Fowler TS, Clayton SD, Riordan JM, Secrist JA. Synthesis and biological activity 2′-fluoro-2-halo-derivatives of 9-β-D-arabinofuranosyladenine. J Med Chem 1992;35:397–401. [PubMed: 1732556]
6. Carson DA, Wasson DB, Esparza LM, Carrera CJ, Kipps T, Cottam HB. Oral antilymphocyte activity and induction of apoptosis by 2-chloro-2′-arabino-fluoro-2′-deoxyadenosine. Proc Natl Acad Sci USA 1992;89:2970–2974. [PubMed: 1348362]
7. Takahashi T, Kanazawa J, Akinaga S, Tamoaki T, Okabe M. Antitumor activity of 2-chloro-9-(2-deoxy-2-fluoro-β-D-arabinofuranosyl)adenine, a novel deoxyadenosine analogue, against human

colon tumor xenographs by oral administration. Cancer chemother Pharmacol 1999;43:233–240. [PubMed: 9923554]

8. Kim CG, Yang DJ, Kim EE, Cherif A, Kuang L, Li C, Tansey W, Liu CW, Li S, Wallace S, Podolof DA. Assessment of tumor cell proliferation using [^{18}F]-fluorodeoxyadenosine and [^{18}F]-fluoroethyluracil. J Pharm Chem 1996;85:339–344.
9. Mikhailopulo IA, Poopeiko NE, Prikota TI, Sivets GG, Kvasyuk EI, Balzirini J, De Clercq E. Synthesis and antiviral and cytostatic properties of 3′-deoxy-3′-fluoro- and 2′-azido-3′-fluoro-2′,3′-dideoxy-D-ribofuranosides of natural heterocyclic bases. J Med Chem 1991;34:2195–2202. [PubMed: 2066992]
10. Van Aerschot A, Herdewijin P, Jansen G, Cools M, De clerq E. Synthesis and antiviral activity evaluation of 3′-fluoro-3′-deoxyribonucleosides: broad-spectrum activity of 3′-fluoro-3′-deoxyadenosine. Antiviral Res 1989;12:133–150. [PubMed: 2624455]
11. Smee DF, Morris JL, Barnard DL, Van Aerschot A. Selective inhibition of arthropod-borne and arenaviruses in vitro by 3′-fluoro-3′-deoxyadenosine. Antiviral Res 1992;18:151–162. [PubMed: 1365816]
12. Robins MJ, Fouron Y, Mengel R. Nucleic acid related compounds. 11. Adenosine 2′, 3′-ribo-epoxide. Synthesis, intramolecular degradation, and transformation into 3′-substituted xylofuranosyl nucleosides and the lyxo-epoxide. J Org Chem 1974;39:1564–1570. [PubMed: 4833508]
13. Lewandowska E, Neschadimenko V, Wnuk SF, Robins MJ. Efficient removal of sugar O-tosyl groups and heterocycle halogens from purine nucleosides with sodium naphthalenide. Tetrahedron 1997;53:6295–6302.
14. Lauer T, Loncar R, Deussen A. Tracer adenosine: A novel myocardial flow marker. J Nucl Med 2003;44:641–648. [PubMed: 12679411]
15. Mathews WB, Nakamoto Y, Ravert HT, Scheffel U, Rauseo PA, Traughber B, Abraham EH, Dannals RF, Wahl RL. ^{11}C-5'-Adenosine monophosphate (^{11}C-AMP): A new radioligand for positron emission tomographic imaging of cancer. J Nucl Med 2002;43:362P.
16. Alauddin MM, Conti PS, Fissekis JD. Synthesis of [^{18}F]-labeled 2′-deoxy-2′-fluoro-1-β-D-arabinofuranosyluracil ([^{18}F]FMAU). J Labelled Comp Radiopharm 2002;45:583–590.
17. Alauddin MM, Conti PS, Fissekis JD. A general synthesis of [^{18}F]-labeled 2′-deoxy-2′-fluoro-1-β-D-arabinofuranosyluracil nucleosides. J Labelled Comp Radiopharm 2003;46:285–289.
18. Alauddin MM, Conti PS, Fissekis JD. Synthesis of [^{18}F]-labeled adenosine analogues as potential PET imaging agents. J Labelled Comp Radiopharm 2003;46:805–814.

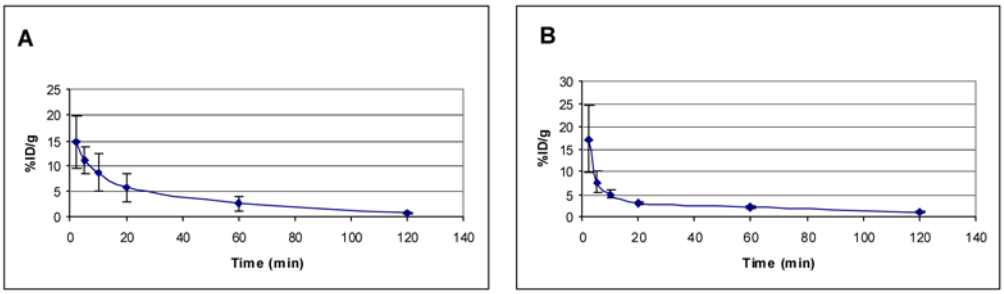

Figure 1.

A: Blood clearance of [^{18}F]FAA, **B:** Blood clearance of [^{18}F]FXA. Mice were injected (i.v) with [^{18}F]FAA or [^{18}F]FAA (~740 MBq). Blood samples were taken (1.33 μL) from the contralateral tail vein at different time points (1, 2, 5, 10, 20, 40, 60 and 120 min). Activity in each blood sample was measured in a gamma counter, standardized and %ID/g was calculated. Mean % ID/g was plotted against time to obtain the blood clearance curve for each compound.

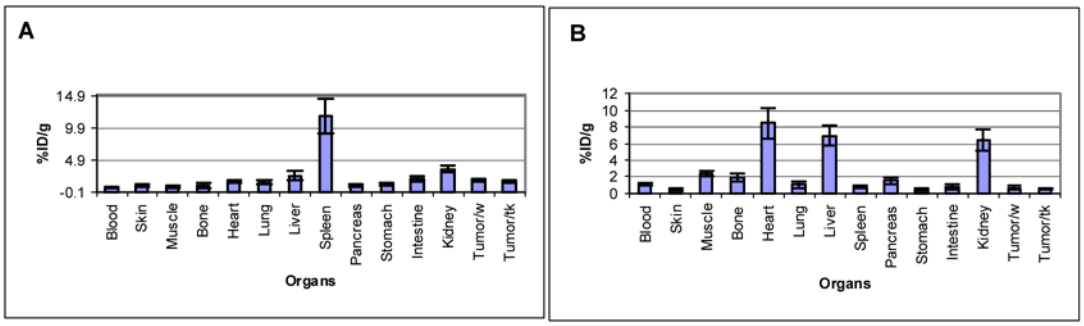

Figure 2.

A: Biodistribution of [^{18}F]FAA, **B:** Biodistribution of [^{18}F]FXA. Animals were injected (i.v) with [^{18}F]-FAA or [^{18}F]-FAA (~740 MBq), anesthetized with Nembutal (40 mg/kg) and sacrificed at 2 h post-injection. Organs including tumor were separated and weighed. Radioactivity in each organ was measured using a gamma counter and radioactivity uptake was expressed as % ID/g and organ to blood ratio.

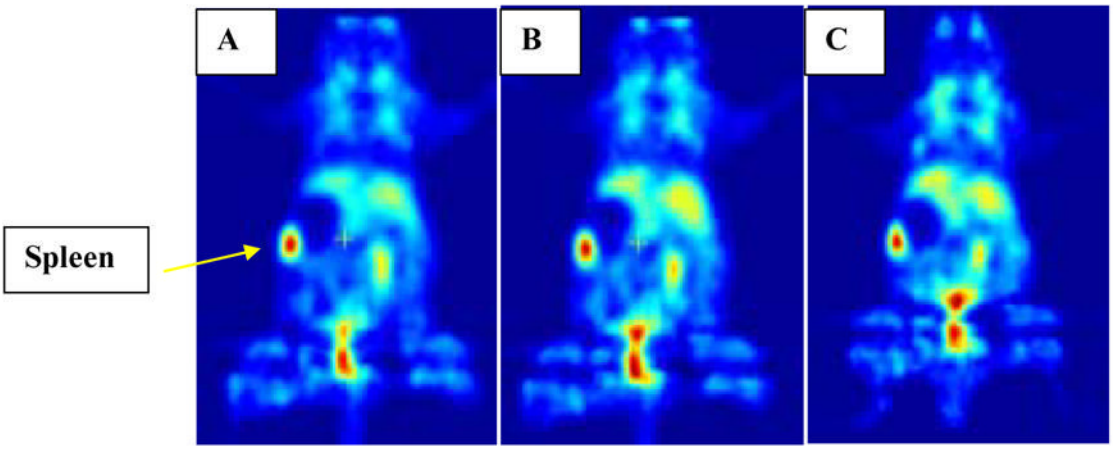

Figure 3.

Micro-PET images of [^{18}F]FAA: Coronal images; **A:** 30 min, **B:** 1h and **C:** 2h post-injection. Animals were injected with [^{18}F]FAA (0.2 mCi, tail vein). PET imaging (10 min static scans) was performed with 120 transaxial planes at 30 min, 1h and 2h post-injection. Images were reconstructed, regional radioactivity concentrations (KBq/cc) were estimated from the maximum pixels within regions of interest drawn around the tumor or organ.

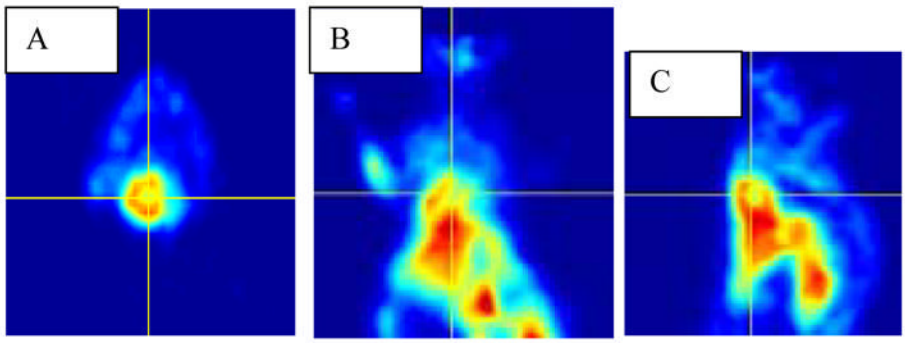

Figure 4.

Micro-PET images of [^{18}F]FXA: **A:** Transaxial, **B:** Coronal and **C:** Sagittal. Animals were injected with [^{18}F]FXA (0.2 mCi, tail vein). PET imaging (10 min static scans) was performed with 120 transaxial planes at 30 min, 1h and 2h post-injection. Images were reconstructed, regional radioactivity concentrations (KBq/cc) were estimated from the maximum pixels within regions of interest drawn around the tumor or organ.

Table 1

Biodistribution of [^{18}F]FAA and [^{18}F]FXA in tumor-bearing animals at 2h post-injection. Animals were injected (i. v.) with [^{18}F]FAA or [^{18}F]FAA (~740 MBq), anesthetized with Nembutal (40 mg/kg) and sacrificed at 2 h post-injection. Organs including tumor were separated and weighed. Radioactivity in each organ was measured using a gamma counter and radioactivity uptake was expressed as % ID/g and organ to blood ratio. Mean uptake (%ID/g) was calculated with standard deviation.

Organs	% ID/g of radiotracers in organs and tumors at 2h			
	% ID/g ([^{18}F]-FAA)	Organ/blood	%ID/g ([^{18}F]-FXA)	Organ/blood
Blood	0.532 ± 0.087	1.00	1.034 ± 0.157	1.00
Skin	1.032 ± 0.214	1.94	0.452 ± 0.146	0.43
Muscle	0.748 ± 0.152	1.41	2.430 ± 0.332	2.31
Bone+marrow	0.908 ± 0.377	1.71	1.844 ± 0.479	1.78
Heart	1.548 ± 0.175	2.91	8.430 ± 1.883	8.15
Lung	1.436 ± 0.311	2.69	1.000 ± 0.401	0.96
Liver	2.433 ± 0.661	4.57	6.934 ± 1.207	6.70
Spleen	11.649 ± 2.698	21.89	0.764 ± 0.160	0.74
Pancreas	0.952 ± 0.158	1.79	1.507 ± 0.334	1.45
Stomach	1.117 ± 0.197	2.09	0.461 ± 0.143	0.44
Intestine	1.926 ± 0.384	3.62	0.726 ± 0.319	0.70
Kidney	3.472 ± 0.500	6.52	6.394 ± 1.241	6.12
Tumor (wild)	1.743 ± 0.242	3.27	0.673 ± 0.168	0.65
Tumor (tk+)	1.554 ± 0.196	2.92	0.489 ± 0.075	0.47

* Average of 5 animals ± SD